Curved X-ray Trajectories in Nonperfect Crystals

B. Dietrich
Akademie der Wissenschaften der DDR, Institut für Physik der Werkstoffbearbeitung Berlin

J. Härtwig *, G. Hölzer, and R. Kittner
Friedrich-Schiller-Universität Jena, Sektion Physik

Z. Naturforsch. **37a**, 638–646 (1982); received March 24, 1982

Dedicated to Prof. G. Hildebrandt on the occasion of his 60th birthday

X-ray trajectories are determined qualitatively and numerically for some one-dimensional deformation gradients by means of Katos geometrical optics.
Based on these results the channelization of X-rays and the X-ray contrast are discussed and proved experimetally.

1. Introduction

In the fifties the interest in investigations of the real-structure of monocrystals increased considerably.

The origin of this tendency has been a result of the fact that with the development of the electronics and the optical industry on one hand the need for the employment of monocrystals grew enormous and on the other hand crystal growth technologies developed rapidly. Thus it was possible to produce growing quantities of more or less perfect synthetic monocrystals. Experimental and theoretical methods to investigate them had to be developed.

The interest in the dynamical theory of X-ray diffraction awakened anew. Besides the investigation of fundamental effects caused by dynamical X-ray diffraction the influence of crystal lattice-distortions on the propagation of X-rays has been studied. One question to be answered was that of the form of X-ray trajectories in weakly deformed crystals. The hypothesis that X-rays travel on curved paths in deformed crystals was tested experimentally and theoretically by Hildebrandt [1] and by Borrmann and Hildebrandt [2].

Only a short time later the theoretical description of the wave field propagation in deformed crystals was developed by Penning and Polder [3], Kato [4], Takagi [5] and Taupin [6].

Reprint requests to Dr. Jürgen Härtwig, Sektion Physik der Friedrich-Schiller-Universität Jena, Max-Wien-Platz 1, DDR-6900 Jena.

The theory of Takagi and Taupin is a detailed wave optical description. Their coupled partial differential equations may be numerically solved in most cases for a given deformation model. On the other hand the geometric optical theory of Kato is a sufficient approximation if one may neglect diffraction effects and has the advantage to give a more obvious understanding of the X-ray propagation and of the contrast formation in the crystal. In some simple cases this theory allows for analytical solutions and gives the possibility of a qualitative discussion of the trajectories and the intensity distribution.

2. X-ray Trajectories in Crystals with x-Depending Deformation Fields

Crystals containing growth striations, growth sector boundaries or diffusion induced concentration gradients of impurity atoms may exhibit displacement fields for which a one-directional variation is a good approximation (i.e. growth striations [7], growth sector boundaries [8], [9]).

Indenbom and Chukhovskij [10] treated the geometrical optics of X-ray beams and showed its analogy to mechanics. For special one-dimensional displacement fields they predicted a channelization and a formation of foci within the crystal.

2.1. Qualitative Determination of X-ray Trajectories

The calculation of trajectories for the symmetrical Laue case starts from Kato's differential

0340-4811 / 82 / 0700-0638 $ 01.30/0. — Please order a reprint rather than making your own copy.

equation [4]:

$$m_0 \frac{\mathrm{d}}{\mathrm{d}z}\left(\frac{v/c}{(1-(v/c)^2)^{1/2}}\right) = \frac{\pi}{c}\left(\frac{\partial^2}{\partial z^2} - c^2\frac{\partial^2}{\partial x^2}\right)(\boldsymbol{g}\cdot\boldsymbol{u}), \tag{1}$$

$$m_0 = \pm\frac{K\sqrt{\chi_g\chi_{\bar{g}}}\,C}{2\sin\theta_\mathrm{B}} = \pm 2\frac{e^2}{m c_\mathrm{e}^2}\frac{F_g}{V_\mathrm{ez}}C\,\mathrm{d}_g$$

$$v = \mathrm{d}x/\mathrm{d}z = \tan\theta\,, \quad c = \tan\theta_\mathrm{B}\,.$$

x points perpendicularly to the reflecting lattice planes, z is parallel to the lattice planes and points towards the crystal.

$K = 2\pi/\lambda$ wave number in vacuum, χ_g g-th Fourier component of polarizability, C polarization factor, e^2/mc_e^2 classic electron radius, F_g structure factor, V_ez unit-cell volume, d_g lattice-plane distance, θ_B Bragg angle, θ angle between trajectory and z axis, $\boldsymbol{g}$ diffraction vector, $\boldsymbol{u}$ displacement vector, m_0 is positive for the weakly absorbed wave field 2, negative for the strongly absorbed wave field 1.

With the x components of the vectors the scalar product on the right handside of (1) takes the form

$$(\boldsymbol{g}\cdot\boldsymbol{u}) = \left(\frac{1}{d_g}\right)u_x\,. \tag{2}$$

By multiplication of (1) with c, rearrangement, with $\mathrm{d}x/\mathrm{d}x$ and differentiation one gets

$$m_0\frac{\mathrm{d}v/\mathrm{d}z}{(1-v^2/c^2)^{3/2}} = \mathrm{c}f(x,z)\,, \tag{3}$$

$$f(x,z) = \frac{\pi}{c}(\partial^2/\partial z^2 - c^2\,\partial^2/\partial x^2)(\boldsymbol{g}\cdot\boldsymbol{u})\,,$$

after Kato "force". (4)

Considering only z independent forces $f(x)$ one may integrate (3):

$$m_0 c^2\,(1/(1-v^2/c^2)^{1/2}) - 1/(1-v_\mathrm{e}^2/c^2)^{1/2} = c_0\int_0^x f(x')\,\mathrm{d}x', \tag{5}$$

$v_\mathrm{e} = \tan\theta_\mathrm{e} = v(x=0, z=0)$ is the initial inclination of the trajectory. The r.h.s. of (5) is the potential of the force $f(x)$ in (4). Resolving v from (5) and introducing the new variable w and the "potential" U by

$$w(x, |v_\mathrm{e}|) = 1/(1-v^2/c^2)^{1/2} \equiv \frac{c\int_0^x f(x')\,\mathrm{d}x'}{m_0 c^2} + 1/(1-v_\mathrm{e}^2/c^2)^{1/2} = -U(x) + w_0 \tag{6}$$

with

$$\frac{c\int_0^x f(x')\,\mathrm{d}x'}{m_0 c^2} = -U(x) + U(0)\,,$$

$$w_0 = U(0) + (1 - v_\mathrm{e}^2/c^2)^{-1/2}$$

one gets

$$\frac{\mathrm{d}x}{\mathrm{d}z} = \pm c\frac{\sqrt{w^2-1}}{w}\,. \tag{7}$$

w_0 is determined by the position of the entrance point in the potential field and by the initial inclination of the ray.

The two signs in (7) are due to the ambiguity of w with respect to v. In (6) it can be seen that

$$w \geqq 1\,. \tag{8}$$

The use of (7) for the inclination of the trajectory with respect to the z-axis is sufficient for the discussion of the qualitative behaviour of the trajectories in a given "potential" $U(x)$ because of the relation

$$U(x) = \frac{\pi}{m_0 d_\mathrm{perf}}\cdot\frac{\Delta d(x)}{d_\mathrm{perf}} \tag{9}$$

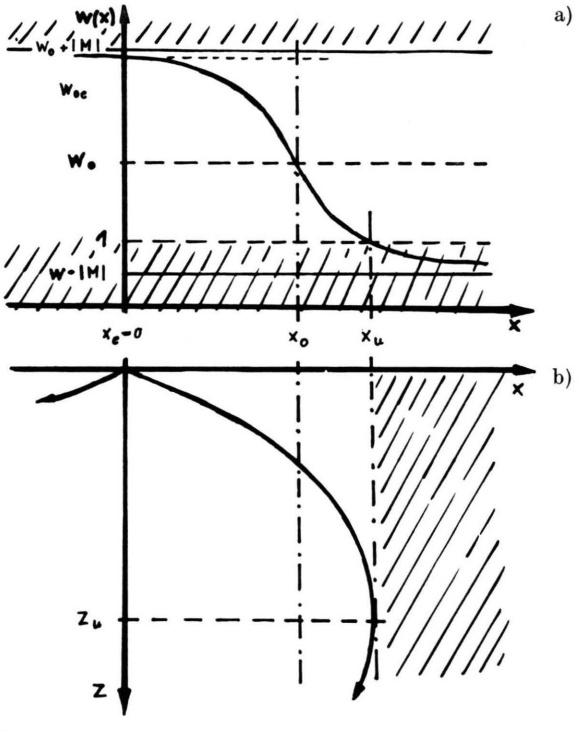

Fig. 1. a) Plot of the quantity $w(x)$ for a step-like potential, b) Two possible trajectories (for one wave field).

for a given relative change of the lattice distance $\Delta d/d$ [11].

A plot of w is shown in Fig. 1 a corresponding to a lattice distance increasing in the x-direction. The two ray trajectories possible for the weakly absorbed wave field are shown in Figure 1 b. In the case of monotonously increasing or decreasing values of $U(x)$ all trajectories have the same sense of curvature. If for example, the potential has the form

$$U(x) = M \tanh \frac{x - x_0}{b}, \tag{10}$$

then it may happen that for a given M and x_0 the quantity v_e reaches values for which the condition (8) cannot be fulfilled for some values of x. This is the case for $w_0 - |M| < 1$. Then we have $w = 1$ for $x = x_u$. The inclination of the ray trajectories becomes zero and thus the trajectories reach a maximum or minimum value of the x-coordinate. The point (x_u, z_u) is then the reversal point of the beam reflected from the potential barrier. The trajectories of the weakly absorbed wave field are obtained for $M > 0$ and those for the strongly absorbed wave field for $M < 0$.

Examples for plots of w in cases of non-monotonously increasing or decreasing potentials are shown in Figs. 2 a and 3 a. In both cases the condition $w_0 - |M| > 1$ is fulfilled and reversal points appear. (The larger $|v_e|$, the higher the plot of $w(x, |v_e|)$ is lying). In one case (Fig. 3 b) the trajectories behave similarly to those in Fig. 1 b, in the other case (Fig. 2 b) a new phenomenon appears. This is the channeling of rays by multiple reflection at the walls of the potential valley.

2.2. *Quantitative Determination of X-ray Trajectories*

Using (7) with a given analytical $U(x)$ to obtain w and $\mathrm{d}x(w)/\mathrm{d}w$ it follows that

$$z(x, |v_e|) = \left| \frac{1}{c} \int_{w(0)}^{w(x)} \frac{w}{(w^2 - 1)^{1/2}} \left(\frac{\mathrm{d}x}{\mathrm{d}w} \right) \mathrm{d}w \right|. \tag{11}$$

with $z_e = 0$.

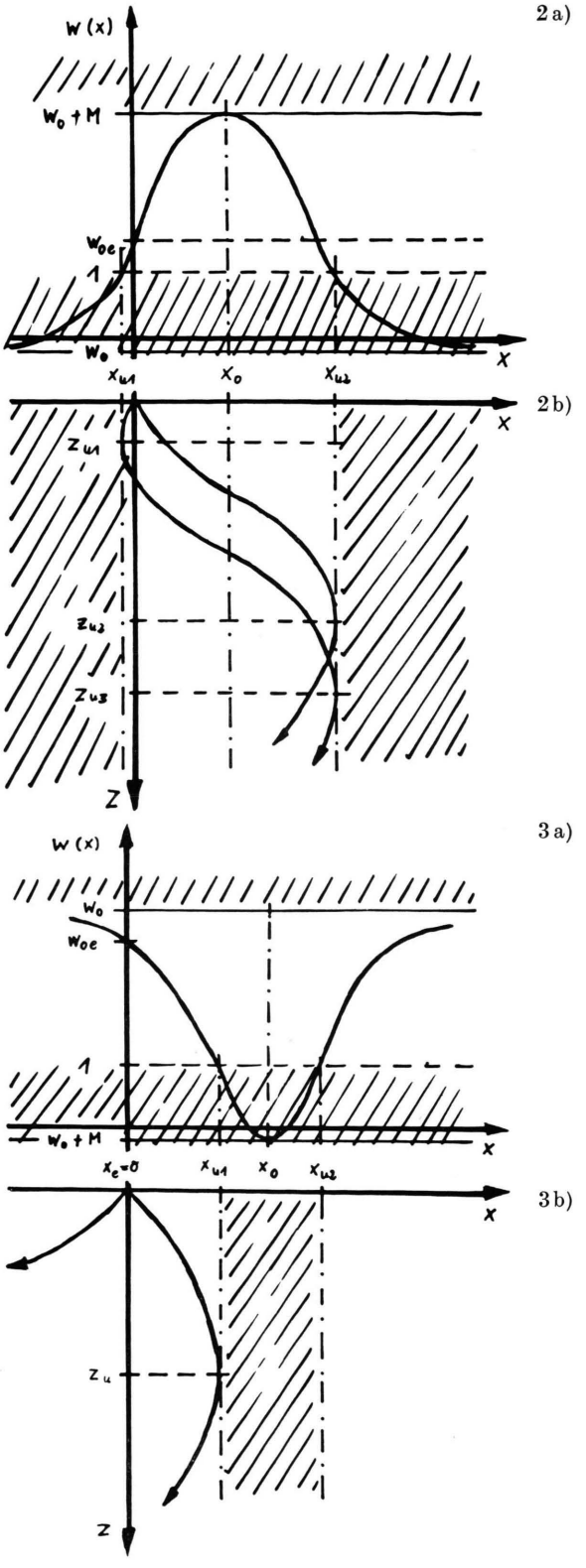

Fig. 2, 3. a) Plot of the quantity $w(x)$ for a potential valley and a potential hill in the case of the weakly absorbed wave field or for a potential valley in the case of the weakly absorbed ($M < 0$) and strongly absorbed ($M > 0$) wave field; b) The possible trajectories.

Equation (11) can be integrated analytically for some special $U(x)$. Some examples are given in [12] and below.

2.2.1. Channelization of X-rays

2.2.1.1. Theoretical Considerations

As it was shown in Fig. 2b, rays starting under angles $\theta_e \leqq \theta_{max}$ may oscillate along the "potential valley" where the angle θ_{max} depends on $w_0 - |M|$. These rays can not leave their valley and guide their energy inside the valley to the exist face, similar to a light guide. These rays are called channelized rays.

Rays starting with small θ_e in the deepest point of the "potential" may form a focus. If the "potential" has for example the form

$$U(x) = M \cos\{(x - x_0)/b\} \tag{12}$$

or

$$U(x) = M/[1 - (x - x_0)^2/b^2], \tag{13}$$

where M, b and x_0 are parameters [12], these "potentials" have a harmonic approximations, so that for $x_0 = 0$, $x/b \ll 1$ and $v_e^2/c^2 \ll 1$ (7) may be integrated from 0 to x_u to obtain constant z_u's:

$$z_u = \frac{\pi}{2} \frac{b}{c\sqrt{M}} \quad \text{and} \quad z_u = \frac{\pi}{4} \sqrt{2} \frac{b}{c\sqrt{M}}, \tag{14}$$

respectively. The distance of the focus from the origin is $2z_u$.

In Figs. 4 and 5 calculated trajectories of the weakly absorbed wave field are shown for the "potential" (12). In Fig. 4 the entrance point lies at a minimum of the potential and in Fig. 5 at a maximum (for the strongly absorbed wave field the two plots have only to be exchanged).

In the case of $\mu z_a > 1$ (μ-linear absorption coefficient) the inner, channelized rays, which form a focus, undergo anomalously weak absorption. Regions of small ray density lie next to the potential valley. If the entrance point lies at a maximum of the potential, all the rays are pushed away from the potential hill and they undergo normal absorption.

2.2.1.2. Experimental Proof

A Czochralski grown single crystal bar of dislocation-free silicon with striation nearly parallel to the (111) face was used to prove the channelization of X-rays [13]. The impurity distribution of Oxygen is almost periodic in the growth direction and changes from the minimum to the maximum by a factor 1.3 to 5 [14].

In the inner part of the crystal the striations are accompanied by an almost periodic variation of the lattice parameter in (111) direction [15, 16].

The potential is proportional to the difference of the lattice parameter to that of the ideal crystal.

A wedge-shaped crystal was cut from the bar as shown in Figure 6. The greatest thickness t was 2 mm and the height h 15 mm. The (111)-reflection and copper radiation were used, suppressing the strongly absorbed wavefield 1.

The contrasts of the section topographs are very sensitive to small shifts of the crystal relative to the primary beam. In the section topograph of Fig. 7 the entrance point lies near to the potential minimum. The very dark streak in the centre marks the trace of the potential valley of the channelized anomalously weakly absorbed rays. The width of the streak depends on the width of the potential valleys.

The existence of the streak may be explained by markedly anomalously weak absorption. Up to now, it has been impossible to show the formation of a focus. This may be caused by the lattice parameter variation of the striations, which is not cosine-like and cannot be described by a harmonic potential near to the minimum.

The section topograph of Fig. 8 was taken after a small shift of the crystal. The entrance point lies at a maximum of the potential now. The rays pushed away from the potential hill undergo normal absorption. No channelized rays of the anomalously weakly absorbed wave field occur. The whole energy of the ray fan is entirely absorbed after a short distance.

2.2.2. X-ray Trajectories for a Step Like Varying Lattice-Plane Distance

For the potential given by (10) the expression (11) can be integrated analytically [12]. Examples of calculated trajectories are shown in Figure 9. The use of known X-ray trajectories lies in the fact that a qualitative discussion of X-ray diffraction contrasts in section topographs is possible on the basis of them.

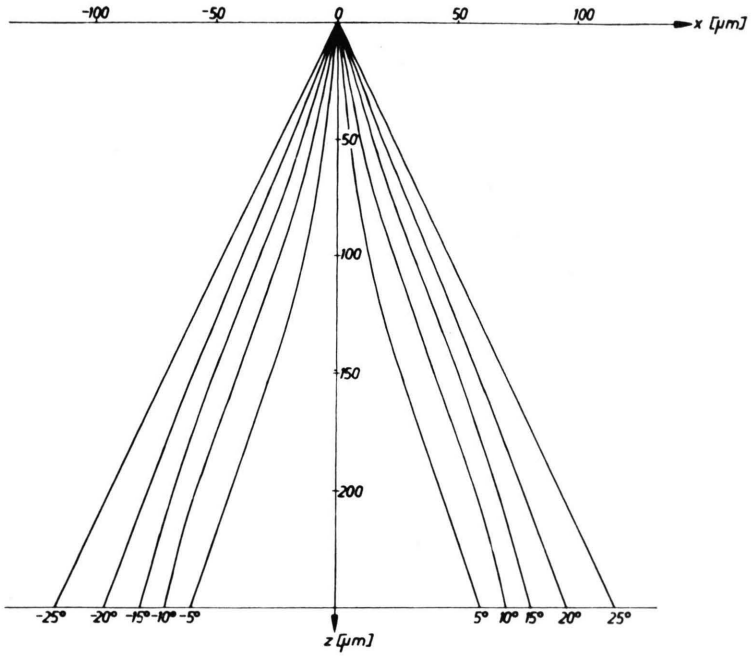

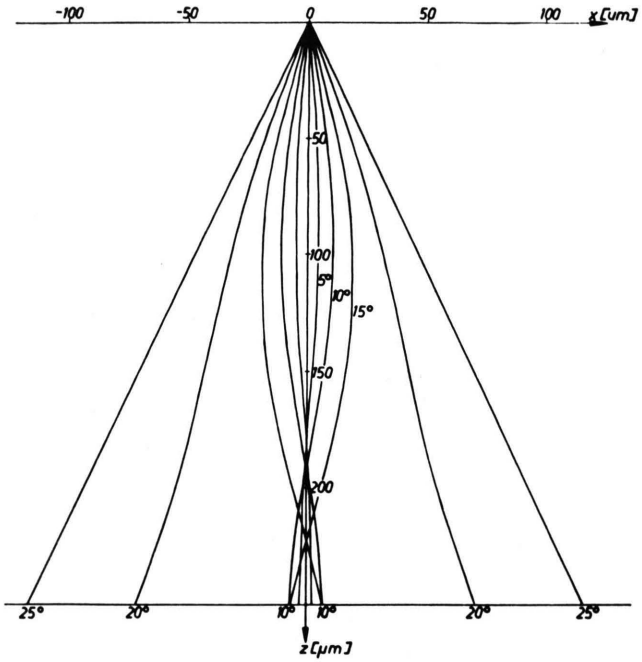

Fig. 4, 5. Trajectories for a cosine like potential. $M = 10^{-6}$. 4: $x_0/b = 0$; 5: $x_0/b = \pi$.

Fig. 5

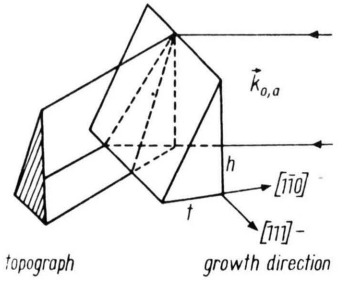

Fig. 6. The wedge shaped crystal and the formation of the section topograph.

Fig. 7. Section topograph, the entrance point lies near the potential minimum.

Fig. 8. Section topograph, the entrance point lies near the potential maximum.

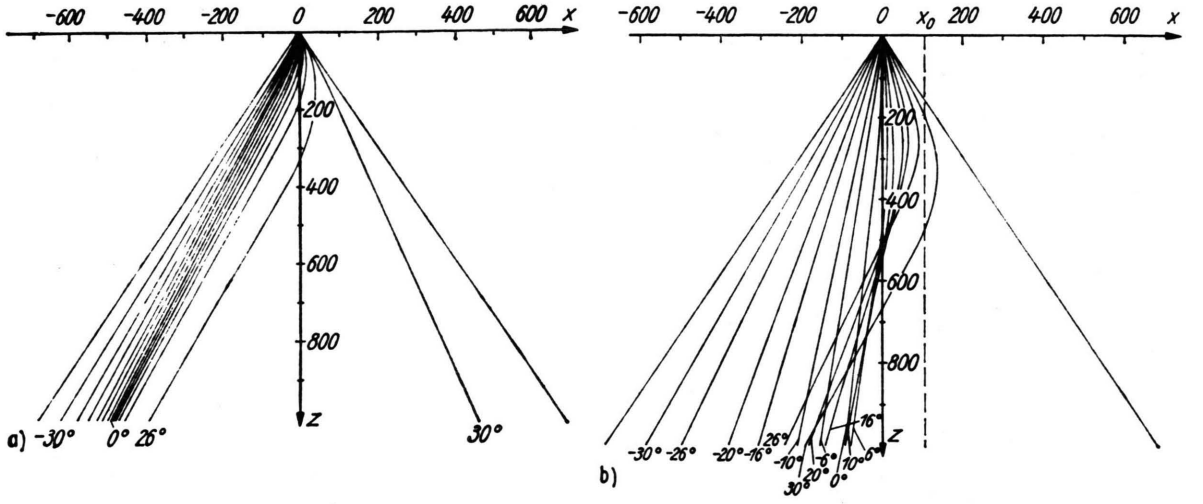

Fig. 9. Trajectories for hyperbolic tangent type potentials. a, b: $M = 10^{-5}$; a: $x_0 = 0$; b: $x_0 = 104$ μm. CuKα$_1$-radiation, $d = 0.137$ nm, $m_0 = 0.201$ μm^{-1}, $b = 50$ μm.

2.3. Possibilities for Analytic Calculations of Intensity Distributions

The calculation of the intensity distribution in section topographs requires the solution of the integrals for the absorption along the rays, the phases and the density of rays on the exit face. All these integrals may be solved analytically in the cases discussed here. But the results for the density of rays is quite intricate. Nevertheless one may discuss the intensity distribution on the base is of the trajectories and the knowledge that strong anomal absorption occurs only for θ near zero, without solving these integrals.

3. Discussion of the Diffracted Intensity

The discussion is restricted to the symmetrical Laue case. It is assumed that the "force" varies so slowly in the x-direction that it does not cause kinematical contrasts.

Following Kato [4] the calculation of the diffracted intensity involves the following steps (Figure 10):

1. Taking account of the boundary condition at the entrance point 0, which gives the intensity of the ray r, starting in 0 with the angle θ,
2. Calculate the trajectory r, which gives the exit point P,
3. calculate the phases and the absorption along the trajectory r,
4. calculate the expansion factor of the trajectories at P, which gives the density of rays at P,
5. consider the boundary condition at P.

To give an idea of the intensity distribution at $z = z_a = t$ the steps 1, 3, 4 and 5 can be discussed qualitatively knowing the X-ray trajectories (step 2) and knowing the following facts [9]:

Under the given restrictions it is permissible to use the boundary conditions of the perfect crystal at 0 and P. Near the entrance surface, the intensity distribution among rays of different initial angles θ is obtained from calculations for the perfect crystal.

They show that the whole ray fan carries energy but the main part propagates near the $\boldsymbol{K}_0$ direction if the divergence of the primary beam is large

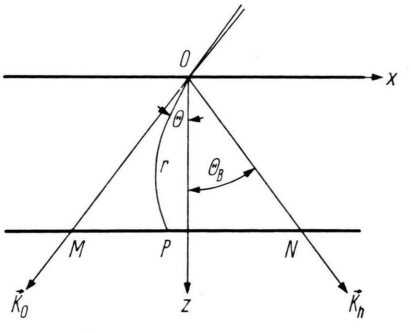

Fig. 10. Propagation of an X-ray beam within the Borrmann fan.

compared with the width of the reflection curve $\Delta\theta_B$.

At the exit surface, the intensity of the rays is distributed between the directions of the rays $\boldsymbol{K}_0$ and $\boldsymbol{K}_h$ outside the crystal. Rays with θ near $-\theta_B(v/c=-1)$ at the exit surface give their energy mainly in the $\boldsymbol{K}_0$ direction, rays with θ near θ_B $(v/c=1)$ mainly in the $\boldsymbol{K}_h$ direction, and rays with $\theta=0\,(v=0)$ divide their energy equally between the $\boldsymbol{K}_0$ and $\boldsymbol{K}_h$ directions.

The absorption along the trajectory gives anomalous weak or strong contributions only for such parts of the trajectories where $|\theta|$ is small, otherwise normal absorption occurs. Therefore in thick crystals only rays with mostly small inclinations $|\theta|$ contribute to the intensity in the topographs.

The phase of rays in the centre of the fan is essentially proportional to the geometrical path.

From a drawing of the trajectories one may also gain an impression of the expansion factor. High energy reaches the exit face at P if trajectories starting under equi-distant θ values are concentrated near P. Thus the trajectories play a central role in the discussion of the intensity distribution.

3.1. X-ray Diffraction Contrast of a Step Like Varying Lattice-Plane Distance

In Fig. 11 the first row shows the x-depending lattice-plane distance, the x dependence of which is proportional to the potential. Below each potential a few ray fans are drawn for different positions of the entrance point 0 in the potential. Only rays are shown which are important for intensity distribution. In the last row, section topographs are sketched for the case where diffracting lattice planes form a small angle with the plane of the centre of the step in the $x-y$ plane. Such an arrangement has the advantage that all the possible positions of the entrance point 0 relative to the centre of the step can be represented in one section topograph.

Here the case $\mu t>1$ will be discussed, where only the weakly absorbed wave field is of importance. The task is to look for anomalously weakly absorbed rays. They may appear if rays propagating initially near the $\boldsymbol{K}_0$ direction and moving towards the step, change their direction after a not too long way within the crystal in such a direction that they form trajectories which are nearly parallel to the

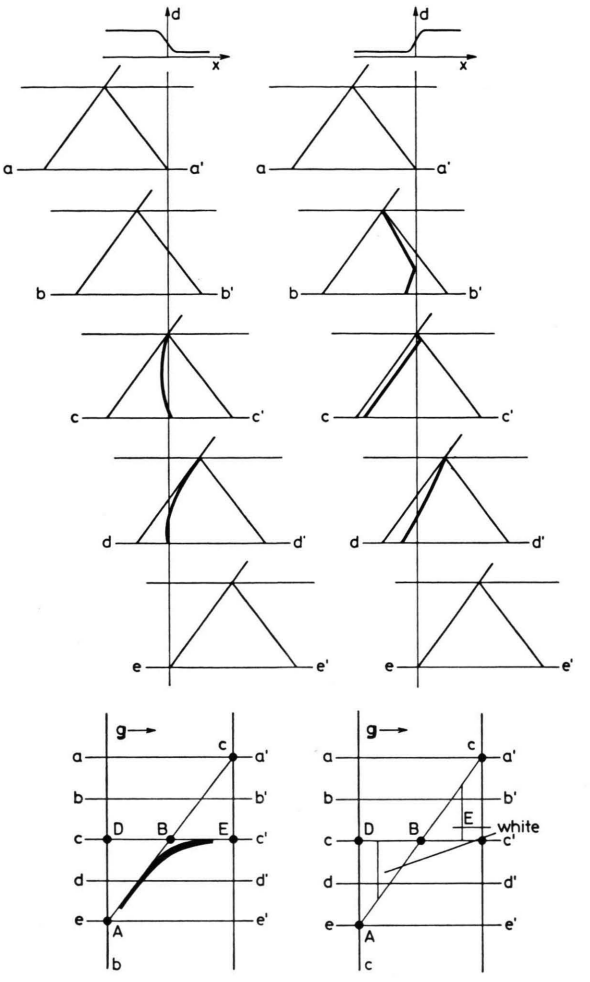

Fig. 11. Construction of the contrast in section topographs with $CuK\alpha_1$ radiation for a steplike varying lattice-plane distance. $\mu t>1$. a: $f>0$; b: $f<0$.

reflecting planes over long distances (Fig. 11a, lines cc′ and dd′). Such trajectories of anomalously weak absorption may be found among those calculated for hyperbolic tangent type potentials. They transfer intensity to the curved line ABE of the section topograph. The blackened area ABE is threefold covered by rays of increasing initial angles (Figure 9b). So one can expect interference effects caused by rays of one wave field only. A more detailed discussion of this problem in the light of the Kato- and Takagi-Taupin-theories, including such questions as the formation and influence of caustics [18] or new wave fields, will be given in a future publication.

Reversing the diffraction vector no excess intensity is transfered to the diffracted beam topograph. In column c of Fig. 2 it is shown that weakly absorbed rays are deflected in the $\boldsymbol{K}_0$ direction by the potential step, which leads to fields ABD and BCE of lowered intensity in the diffracted beam topograph.

3.2. Experimental Proof

To prove the ideas outlined above a crystal was prepared with a step-like varying lattice-plane distance. A quartz crystal of low dislocation density was used.

The step of the lattice plane distance was introduced by interruption of the growth process, after polishing and etching the z-growth surface the growth was continued under different conditions. An X-plate (1 mm thick) was cut from this sample containing a lattice-plane distance which exhibits a step-like variation in the crystallographic c direction. Section topographs of the $(0\bar{2}23)$ plane, forming an angle $\varphi = 40.3°$ with the (0001) plane, were taken by $CuK\alpha_1$ radiation of a Rigaku RU 200 rotating-anode generator (Figure 12). The contrasts of the topographs correspond well to the results of the discussion (Figure 12).

Epelboin [17] has studied theoretically the topographic contrast of a stacking fault in the Laue-Bragg case by a qualitative discussion and by computation. A stacking fault is characterized by a well defined value of the displacement component u_x between the parts of the crystal separated by the fault plane. This corresponds to a δ-function like potential. Some kind of similarity therefore exists to the step-like potential discussed here. In the case of strong absorption we found interference fringes (Figure 12). They are similar to those for a stacking fault in the Laue-Bragg case found by Epelboin ([17], Fig. 8) but in the case of low absorption and

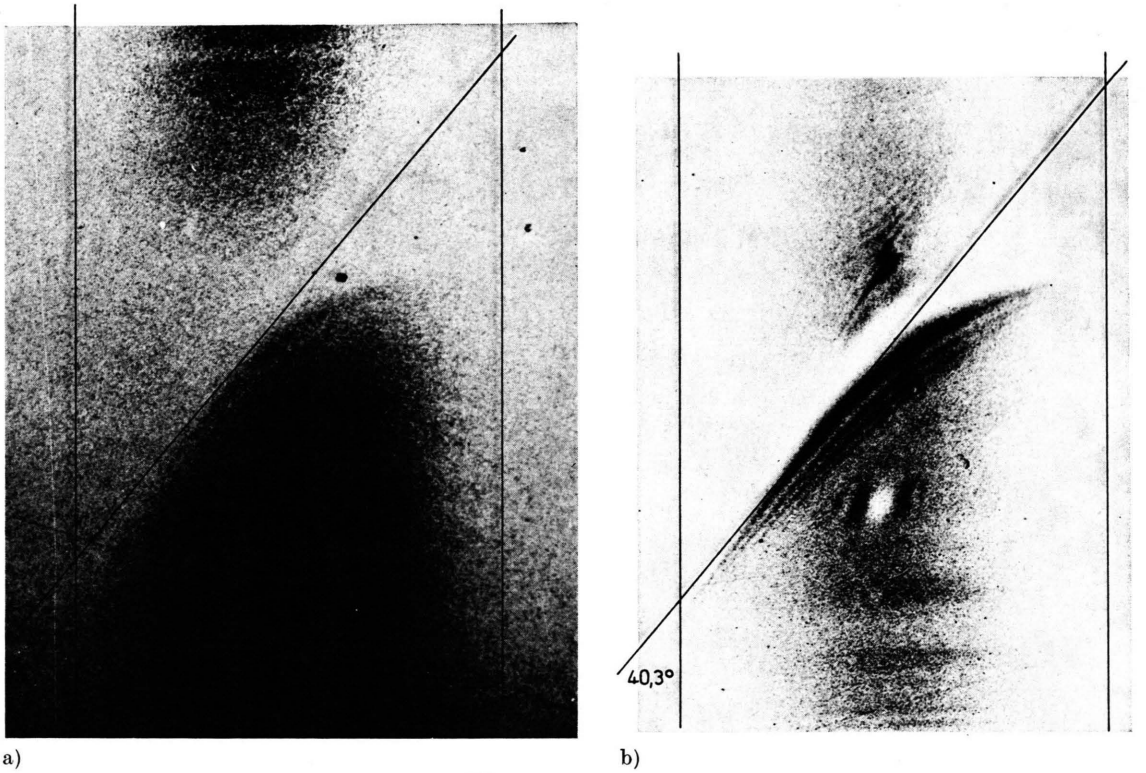

Fig. 12. Observed contrast in the section topographs of the $(0\bar{2}23)$ reflection with $CuK\alpha_1$ radiation. The lattice parameter decreases (a) and increases (b) in direction of the diffraction vector.

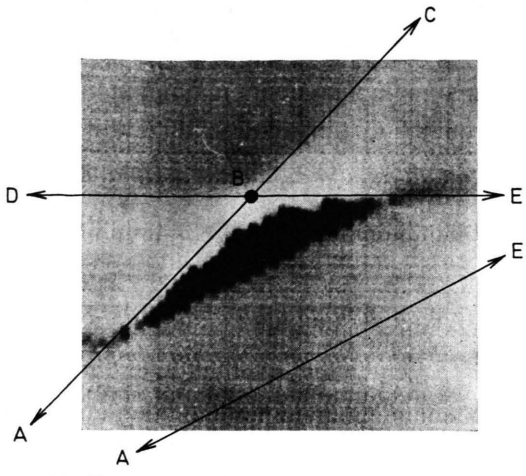

Fig. 13. Computer simulation of a section topograph with $CuK\alpha_1$ radiation for a step-like varying lattice-plane distance. $b = 10$ μm, $M = 2 \cdot 10^{-6}$ (the letters A to E indicate the same points like in Figure 11).

they are due to interferences of rays of the weakly absorbed wave field only, running different ways, and due to the creation of new wave fields by this wave field.

A computer simulation of a section topograph according to the experimental conditions of Fig. 12a calculated using the Kato-theory for a step like potential is shown in Figure 13.

The parameters b and M are not fitted well yet (b too large, M too small) but a rather good agreement with the qualitative discussion and the experimental result can be stated.

4. Final Observation

The experimental demonstration of the curvature of X-ray trajectories by deformation gradients and the Eikonal theory of X-ray propagation evaluated by Kato are the basis of the outlined analytical solutions and of their image. Substantial parts of topographic contrasts were discussed qualitatively in a few examples. In addition to the possible computer simulation of contrasts in section topographs, the interpretation of the intensity distribution by a mechanical analoge has the advantage of forming a simple idea of the contrast and may be used to evaluate models of deformation fields.

[1] G. Hildebrandt, Z. Kristallogr. **112**, 312, 340 (1959).
[2] G. Borrmann and G. Hildebrandt, Z. Physik **156**, 189 (1959).
[3] P. Penning and D. Polder, Philips Res. Repts. **16**, 419 (1961).
[4] N. Kato, J. Phys. Soc. Japan **18**, 1785 (1963); **19**, 67, 971 (1964).
[5] S. Takagi, Acta Cryst. **15**, 1311 (1962).
[6] D. Taupin, Bull. Soc. Fr. Minéral. Cristallogr. **87**, 469 (1964).
[7] B. Jenichen and R. Köhler. Phys. stat. sol. (a) **65**, 245, 535 (1981).
[8] J. Härtwig, Cryst. Res. Technol. **16**, 1297 (1981).
[9] B. Dietrich, J. Härtwig, A. Christoph, and G. Hölzer, Phys. stat. sol. (a) **63**, 511 (1981).
[10] W. L. Indenborn and F. N. Chukhovskij, Kristallografija **16**, 1101 (1971).
[11] B. Dietrich and J. Härtwig, Cryst. Res. Techn. **16**, 931 (1981).
[12] B. Dietrich and J. Härtwig, Krist. Techn. **15**, 1377 (1980).
[13] B. Dietrich and R. Kittner, Phys. stat. sol. (a) **60**, K 5 (1980).
[14] P. Gaworzeski, S. Hähle, and H. Riemann, Krist. Techn. **12**, 871 (1977).
[15] A. Fukuhara and Y. Takano, Acta Cryst. A **33**, 137 (1977).
[16] A. J. R. De Kook, P. J. Roksnoer, and P. G. T. Bonnen, J. Crystal Growth **28**, 125 (1975).
[17] Y. Epelboin, J. Appl. Phys. **50**, 1312 (1979).
[18] K. Kambe, Z. Naturforsch. **18a**, 1010 (1963).